Multi-Person Respiratory Monitoring Using Single-Channel Continuous-Wave Radar with Time Modulated Array

Lei Guan, Tong Wu, Xiaodong Yang, Nan Zhao, Zhiya Zhang, Akram Alomainy, Muhammad Ali Imran,

Qammer H. Abbasi

***Abstract*—Radio frequency (RF) signals are widely used in respiratory detection due to their non-contact, remote sensing advantages. In order to satisfy multi-person monitoring, the existing RF sensing system greatly increases the complexity of the feeder network, which will affect the stability of the system and have high maintenance costs. In this study, we propose a single-channel, low-complexity multi-person respiratory monitoring system. It uses a time modulated array (TMA) to detect the position and respiration rate of multiple targets. The TMA is reconstructed into a conventional multichannel array by the harmonic recovery method. Beamforming is used to scan the scene horizontally. At the same time, the beamformed signal is converted to the frequency domain to construct the angle of arrival-frequency map (AFM). By forming a beam pointing to the target, the time domain respiration signal of each target can be acquired. The experimental results show that the maximum RR estimation errors of the proposed system in single-person, two-person, and three-person scenarios are 0.77 bmp, 0.96 bmp, and 1.32 bmp, respectively. In addition, the Bland-Altman analysis shows that our system has good consistency with the reference sensor.**

***Index Terms*— TMA, multi-person, respiratory monitoring.**

I. INTRODUCTION

Respiratory rate (RR) is an important physiological assessment indicator for health status [1]. Accurate measurement of the RR is essential for vital signs monitoring of patients with breathing troubles such as chronic obstructive pulmonary disease (COPD). Daily respiratory monitoring in a consistent and cost-effective manner plays an important role in assessing patient progress and treatment, especially in the case of the COVID-19 global pandemic.

Traditional wearable breath sensors such as capnography or impedance pneumography are widely used in the medical field, but these technologies can cause discomfort/injury to patients, especially in the case of skin burns, premature birth, and skin diseases. The solution based on computer vision can non-invasive detect the vital signs of targets [2-3]. However, there is a risk of privacy leakage from video-recorded images. In addition, light intensity affects the performance of the system. RF sensing schemes are the most promising candidates to overcome these drawbacks. The low-power radars [4-5] and fast vital sign estimation methods [6-7] are proposed for continuous monitoring. In vital sign measurement, the phase is affected by hardware noise and environmental noise. The adaptive variational mode decomposition (VMD) [8,9] are proposed for separating respiratory and heartbeat signals, which significantly improves the signal-to-noise ratio (SNR). In addition, RF signals can be applied in scenarios such as non-line-of-sight sensing [10], through-wall monitoring [11-12], and disaster rescue [13] due to their reflection and penetration characteristics. However, the above research only focuses on extracting vital signs from single target.

In a multi-target detection scenario, multiple targets simultaneously affect the RF signal. Therefore, the receiver needs to have the ability to separate the individual targets from the mixed signal. Currently, there are four main solutions to detect the vital signs of multiple targets: frequency separation, distance separation, spatial separation and blind signal separation (BSS). Assuming that the RR of different people is distinct, the RR of each person can be obtained in the frequency domain. TR-BREATH [14] projects WiFi channel state information (CSI) into the time inverted resonance intensity feature space and then applies the root-MUSIC algorithm to estimate the respiratory rate of multiple targets. TensorBeat [15] employes CSI phase difference data to obtain the periodic signals from the movements of multiple breathing chests by leveraging tensor decomposition. These methods require the number of targets as prior knowledge which is not applicable in practical scenarios. Moreover, the performance degrades when the RR difference between two targets is less than the frequency resolution.

For the solution based on distance separation, targets can be separated depending on the inherent range resolution of the radar. The impulse-radio ultrawideband (IR-UWB) radar transmits a pulse signal and obtains range information on subjects from the propagation delays of echo signals [16-18]. Although IR-UWB radars provide higher range resolution with their large bandwidth, it is very challenging to generate high power pulses in the wide band. This leads to a trade-off

Lei Guan, Tong Wu, Xiaodong Yang, Nan Zhao, Zhiya Zhang are with the School of Electronic Engineering, Xidian University, Xi'an, Shaanxi, China, 710071.

Akram Alomainy is with the School of Electronic Engineering and Computer Science, Queen Mary University of London, London E1 4NS, UK.

Muhammad Ali Imran and Qammer H. Abbasi are with the James Watt School of Engineering, University of Glasgow, Glasgow, G12 8QQ.

between range resolution and maximum range [27]. The frequency-modulated continuous wave (FMCW) [19-24] and stepped frequency continuous wave (SFCW) [25-29] can also separate multiple targets based on different radial distances from each target to the radar. When the radial distance between two targets is less than the range resolution, the conventional FFT-based method cannot resolve multiple targets due to the overlap of the main lobes of the sinc function. Super-resolution algorithms such as MUSIC are used to improve range resolution [23], but the performance of the MUSIC algorithm depends on the number of targets, number of snapshots, and system SNR. Li et al. overcame this problem by reconstructing 3D images using frequency-domain back projection (BP) algorithm for the spatial positioning of each target [28]. However, they still cannot separate the respiration of multiple subjects at the same range.

According to the different spatial distributions of multiple targets, matching algorithms and beamforming can be used to separate multiple targets. VSign-ID utilizes the echo signals of multiple self-injection-locked (SIL) radars to mark each person's vital signs on a thermal image through spatial and temporal matching [30]. The several approaches to beam steering include leaky wave antennas, phased arrays, and digital beamforming (DBF). The leaky-wave antenna realizes regular and large-range beam scanning by changing the frequency of the RF signal [31,32]. Although these architectures have low hardware complexity, the angular resolution depends on the antenna pattern. In [33], phased array radar is explored for multi-person breathing. The system uses the phase shifter to control the phase of each RF channel to achieve beamforming. Its flexibility and accuracy are lower than DBF. Therefore, DBF is the mainstream technology for multi-target detection. Xiong et al. proposed a single-input–multiple-output (SIMO) CW radar with adaptive DBF for simultaneous detection of multiple breaths [34]. In [35], a time division multiple-input–multiple-output (MIMO) radar uses 2D digital beamforming to image the chest of multi-target to obtain vital signs. Su et al. propose a Doppler-weighted range-azimuth map to improve the spatial resolution [36]. However, these systems are bulky volumes and have complex feed networks and control circuits. Virtual antenna technology is proposed to improve the aperture and spatial resolution of TI millimeter wave radar [37-39]. However, the millimeter wave penetration performance is poor. If the target's clothes are thick, the detection accuracy will decrease.

According to the statistically independent reflection signals of the targets, the multi-person respiration sensing can be modeled as a BSS problem and solved by the independent component analysis (ICA) method [40-41]. Unfortunately, the solution of ICA needs to know the number of targets. In order to overcome this problem, Zhang et al. present underdetermined BSS approach to separate the respiratory signal of multiple targets without predetermining the number of targets [42]. However, the separated signals are difficult to correspond to each target.

Most of the previous multi-person respiratory detection systems have high hardware complexity and complex control circuits. The performance of the single-domain (distance domain, angle domain) target separation method is limited by the inherent resolution of the radar. To address the above issues, we propose a TMACW radar. A single-channel TMA reduces RF links and hardware costs [43]. The TMA is also used for direction finding [44] and target localization [45] due to its simple architecture. In addition, DBF and FFT are used to map the multi-target echo data into AFM. The main contributions of this paper are as follows.

1. To the best of our knowledge, this is the first system to monitor multi-target respiration using TMA. Specifically, the harmonic recovery technology is used to convert TMA into the conventional multichannel array which reduces hardware complexity.

2. We propose a method for joint spatial domain and frequency domain estimation of multi-person RR, which improves the ability of multi-target separation and anti-interference.

3. We built a prototype of TMACW radar and performed extensive experiments to evaluate the performance of the system. The experimental results show that the proposed system is highly consistent with the reference sensor.

This paper is organized as follows. Section II introduces the system architecture, the multi-person respiratory sensing model based on TMA, and signal processing methods. Section III presents the results and discussions. Finally, the conclusions are drawn in Section IV.

II. METHODOLOGY

A. System Architecture and Hardware

The architecture of the proposed system is shown in Fig. 1. The system consists of TMACW radar and signal processing module. First, the TMACW radar acquires the target echo and converts it to baseband. Then, the digital down-conversion (DDC) filter group is used to extract the required harmonic components. The proposed harmonic recovery method transforms TMA into the conventional multichannel array. DBF forms spatially distributed beams to scan the region of interest horizontally. After eliminating static clutter, FFT is performed on each beam to construct AFM. Finally, the AOA and RR of each target can be obtained from the AFM.

In general, there are two main schemes for the development of radar systems: modular assembly and software defined radio (SDR)-based method. The concept of SDR programmability provides convenience in the development and optimization of radar systems. Previous studies have utilized various SDR devices to implement radar systems [46,47]. Inspired by the above research, we developed the TMACW radar prototype using off-the-shelf control circuits and data acquisition instruments as shown in Fig. 2. The system consists of a transceiver, a single-pole-four-throw (SP4T) RF switch (HMC7992), five microstrip Yagi antennas with 6 dBi gain and an external MCU. Specifically, we use a USRP B210 from Ettus Research as the transceiver to quickly validate the proposed method. The flow graph is deployed in the free and open source GNURadio framework, which reduces the technical requirements for system development. The single-channel TMA consisting of four antennas and HMC7992 switch is connected to the USRP B210 receiving

channel for obtaining target echoes. We use a STM32F103ZET6 (STM32) board to serve as the external MCU with its GPIO to control the HMC7992 switch. The two GPIO pins of STM32 are connected to a two-pin voltage CMOS control interface of HMC7992 in order to turn on and off each channel of the switch in turn. It is worth noting that the TMA in this study works in the receiving state. Therefore, it will not radiate infinite harmonics into space, occupy a large amount of frequency spectrum and interfere with nearby communication equipment.

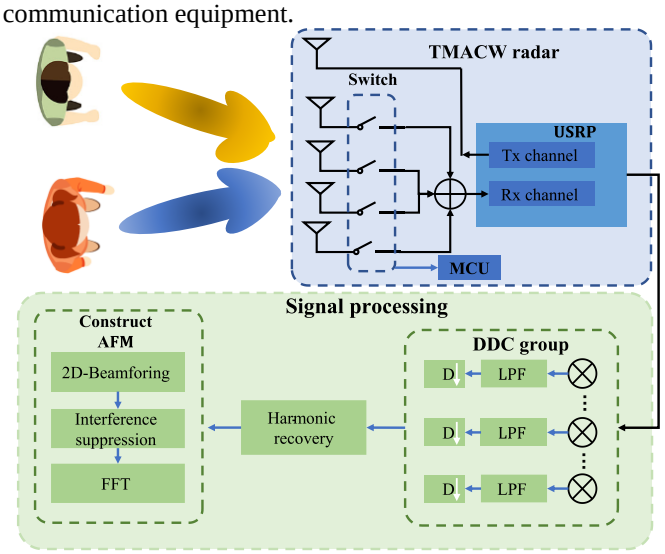

Fig. 1. System architecture.

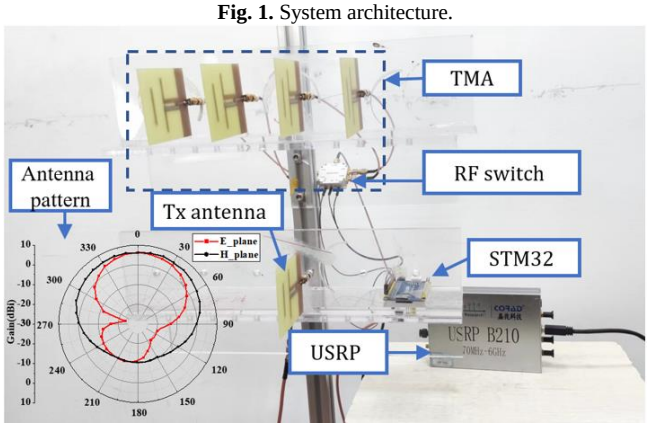

Fig. 2. Prototype of the proposed TMACW radar.

B. Sensing Model Based on TMA

The CW signal sent by the transmitter is reflected by surrounding objects and then returned to the receiver. For the uniform linear array (ULA), the signals traveling via multipath transmission obtained by the *n*th antenna can be expressed as:

$$x_n(t)=\sum_{i=1}^{L}\alpha_i e^{-j2\pi f_c\tau_i}e^{-j(n-1)d\beta\sin\theta_i} \tag{1}$$

where f_c denotes the carrier frequency of the transmitted signal, L is the number of objects or targets, $\tau_i(t)$ the propagation delay to the first antenna of the ith object echo, β is the spatial wavenumber of the carrier frequency f_c, d is spacing between two adjacent antennas, θ_i is AOA of the ith object and α_i is echo amplitude related to the propagation loss and the reflectivity of the ith object.

In fact, the received signal includes the dynamic components of human motion and the static components reflected by static objects, so (1) can be rewritten as:

$$\begin{aligned}x_n(t)&=\sum_{i=1}^{K}\alpha_{i,n}e^{-j2\pi f_c\tau_i}e^{-j(n-1)\beta d\sin\theta_i}+\sum_{m=1}^{M}\alpha_{m,n}e^{-j2\pi f_c\tau_m(t)}e^{-j(n-1)\beta d\sin\theta_m}\\&=x_n^S+x_n^D(t)\end{aligned} \tag{2}$$

where K and M represent the number of stationary objects and moving targets, respectively. x_n^S and $x_n^D(t)$ are the static components and the dynamic components, respectively. If we only consider the dynamic components caused by respiration, the time delay $\tau_m(t)$ is expressed as follows:

$$\tau_m(t)=\frac{2\left(d_{0,m}+d_{r,m}\sin\left(2\pi f_m t+\varphi_m\right)\right)}{c} \tag{3}$$

where $d_{0,m}$ is the distance from the mth target to the ULA, $d_{r,m}$ is the displacement of chest wall of the mth target, f_m and φ_m is respiratory rate and initial phase. The TMA can be obtained by periodic modulation of an ULA. Specifically, a periodically controllable switch is added to each element. In the proposed TMACW radar, the received signal should be rewritten as:

$$y(t)=\sum_{n=1}^{N}U_n(t)x_n(t) \tag{4}$$

where $U_n(t)$ is the modulation function of the nth element. $U_n(t)$ is determined by the time modulation method, the common time modulation methods are variable aperture sizes, unidirectional phase center motion, bidirectional phase center motion, pulse shifting (PS) and sub-sectional optimized time steps. This paper takes PS modulation as an example to introduce the application of time modulation array in respiratory monitoring. The function $U_n(t)$ is shown in Fig. 3 and can be expressed as below:

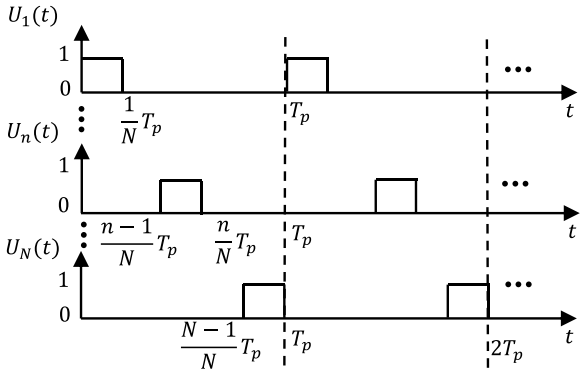

Fig. 3. Periodical modulation function $U_n(t)$, n = 1,2, …, N.

$$U_n(t)=\begin{cases}1, & \left(m+\dfrac{n-1}{N}\right)T_p<t<\left(m+\dfrac{n}{N}\right)T_p\\ 0, & others\end{cases} \tag{5}$$

where T_P is the modulation period. Because the modulation function $U_n(t)$ is periodic, $U_n(t)$ can be expanded by Fourier series:

$$U_n=\sum_{k=-\infty}^{\infty}a_{n,k}e^{j2\pi kf_p t} \tag{6}$$

where $f_p = 1/T_P$ is the modulation frequency. The kth harmonic coefficient $a_{n,k}$ can be expressed as:

$$\begin{aligned} a_{n,k} &= \frac{1}{T_p}\int_0^{T_p} U_n(t) e^{-j2\pi k f_p t} \\ &= \frac{1}{T_p}\int_{t_{on,n}}^{t_{off,n}} e^{-j2\pi k f_p t} \\ &= \begin{cases} \dfrac{\sin\left(\pi k f_p\left(t_{off,n}-t_{on,n}\right)\right)}{\pi k} e^{-j\pi k f_p\left(t_{off,n}+t_{on,n}\right)}, & k\neq 0 \\ f_p\left(t_{off,n}-t_{on,n}\right), & k=0 \end{cases} \end{aligned} \tag{7}$$

where $t_{on,n} = (n\text{-}1)T_p/N$ and $t_{off,n} = nT_p/N$ represent the turn-on time and turn-off time of the nth RF switch, respectively. Inserting (4) and (5) into (2), the single-channel signal after modulation can be written as:

$$\begin{aligned} y(t) &= \sum_{n=1}^{N} U_n(t) x_n(t) \\ &= \sum_{n=1}^{N}\left(\sum_{k=-\infty}^{\infty} a_{n,k} e^{j2\pi k f_p t}\right) x_n(t) \\ &= \sum_{k=-\infty}^{\infty} e^{j2\pi k f_p t}\left(\sum_{n=1}^{N} a_{n,k} x_n(t)\right) \end{aligned} \tag{8}$$

After time modulation, the signal received by a single channel is the sum of the fundamental component and the harmonic components of each order. In the spectrum, it is equivalent to shifting the fundamental component at an interval of f_p as shown in Fig. 4.

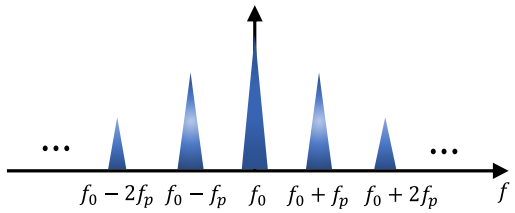

Fig. 4. The Spectrum diagram of TMA.

C. Recovery of Conventional Arrays

The baseband signal consists of an infinite number of harmonics, and the frequency spacing between adjacent harmonics is fp. We can use a series of DDC to move each harmonic component to baseband, then the digital domain of the kth harmonic is expressed as:

$$y_k(t_q) = \sum_{n=1}^{N} a_{n,k} x_n(t_q) \tag{9}$$

Add noise to the model and rewrite (9) as a matrix form, shown as:

$$\begin{aligned} \boldsymbol{Y}(t_q) &= \boldsymbol{\Gamma}\left(\boldsymbol{X}(t_q) + \boldsymbol{N}(t_q)\right) \\ &= \boldsymbol{\Gamma}\boldsymbol{X}(t_q) + \boldsymbol{N}'(t_q) \end{aligned} \tag{10}$$

where $\boldsymbol{Y}(t_q)=[y_{-K}(t_q), y_{-K+1}(t_q), \ldots, y_K(t_q)]^T$ is the harmonic matrix, $\boldsymbol{X}(t_q)=[x_1(t_q), x_2(t_q), \ldots, x_N(t_q)]^T$ is the baseband signal received by each element, $\boldsymbol{N}'(t_q) = [n_{-K}(t_q), n_{-K+1}(t_q), \ldots, n_K(t_q)]^T$ is the noise matrix and $\boldsymbol{\Gamma} \in \mathbb{C}^{2N\times(K+1)}$ is harmonic coefficient matrix and is given by:

$$\boldsymbol{\Gamma} = \begin{bmatrix} a_{-K,1} & a_{-K,2} & \cdots & a_{-K,N} \\ a_{-K+1,1} & a_{-K+1,2} & \cdots & a_{-K+1,N} \\ \vdots & \vdots & \ddots & \vdots \\ a_{K,1} & a_{K,2} & \cdots & a_{K,N} \end{bmatrix} \tag{11}$$

In order to recover the same receiving signals as conventional arrays from the harmonic components, the recovery can be transformed into solving the unconstrained norm approximation problem:

$$\min_{\mathbf{x}(t_q)} \left\| \boldsymbol{\Gamma}\boldsymbol{X}(t_q) - \boldsymbol{Y}(t_q) \right\| \tag{12}$$

where $\|$ is a norm on $\mathbb{C}^{2K+1}$. When $(2K+1) \geq N$, which means $\boldsymbol{\Gamma}$ is column full rank, the best-fit solution can be obtained applying complex least square:

$$\boldsymbol{X}(t_q) = \left(\boldsymbol{\Gamma}^H\boldsymbol{\Gamma}\right)^{-1}\boldsymbol{\Gamma}^H\boldsymbol{Y}(t_q) \tag{13}$$

where superscript H indicates the conjugate transpose operation, $\boldsymbol{X}(t_q)$ is the recovered signal of TMA. In this study, the number of antennas N=4, then the traditional array can be restored when $K \geqslant 2$, which means that we only need to extract ± 2, ± 1 order harmonics and fundamental waves.

D. Construct AFM

With (13), the original signal matrix can be estimated successfully from the modulated single-channel signal. Spatial spectral estimation methods can be used to estimate the target. Considering the lack of information such as the number and location of targets, we use conventional beamforming method to scan the space horizontally. For an arbitrary signal arrival angle θ, the steering vector is expressed as:

$$w(\theta) = \left[1, e^{j\beta d\sin\theta}, \ldots, e^{j(N-1)\beta d\sin\theta}\right] \tag{14}$$

By computing the weighted sum of signals received by all antennas, the beamformed signal is expressed as:

$$\begin{aligned} y(\theta, t_q) &= w(\theta) X \\ &= w(\theta)\left(X^D + X^S\right) \\ &= \underbrace{w(\theta) X^D}_{\text{Static components}} + \underbrace{w(\theta) X^S}_{\text{Dynamic components}} \end{aligned} \tag{15}$$

where $X^D = [x_1^D(t_p), x_2^D(t_p), \ldots, x_N^D(t_p)]^T$ is the static components vector, $X^S = [x_1^S(t_p), x_2^S(t_p), \ldots, x_N^S(t_p)]^T$ is the dynamic components vector. Where $\theta = \theta_m$, the breath signal of the mth target output by the beamformer reaches the maximum and is denoted as $\sum_{n=1}^{N} \alpha_{m,n} e^{-j2\pi f_c \tau_m(t_q)}$. Similarly, when $\theta = \theta_i$, that is, there is no moving target in this direction. The reflected signal of static target reaches the maximum and is denoted as $\sum_{n=1}^{N} \alpha_{i,n} e^{-j2\pi f_c \tau_i}$. If the strength of the static reflection signal is much greater than that of the human body, it will be difficult to find the desired target from the spatial spectrum. Considering from the frequency domain, when there is only a static target in the scanning direction, the energy of the beamformed signal is mainly concentrated in the zero frequency. The beamformed signal will generate a corresponding peak in the frequency spectrum if there is a moving target in the direction. Based on the above analysis, we can find spectral lines of regular chest wall motion in the spectrum by performing FFT on the beamformed signal. In

order to obtain the spectral information of the target, we need to further analyze the dynamic components.

$$\sum_{n=1}^{N} a_{m,n} e^{j2\pi f_c \tau_m(t_q)} = \sum_{n=1}^{N} a_{m,n} e^{\frac{-j4\pi\left[d_{0,m}+d_{r,m}\sin\left(2\pi f_b t_q+\varphi\right)\right]}{\lambda}} = \underbrace{\sum_{n=1}^{N} a_{m,n} e^{\frac{-j4\pi d_{0,m}}{\lambda}}}_{①} \times \underbrace{e^{\frac{-j4\pi d_{r,m}\sin\left(2\pi f_b t_q+\varphi\right)}{\lambda}}}_{②} \quad (16)$$

where the term ① can be regarded as a constant, and the term ② contains the respiratory signal of interest. According to the Jacobi-Anger expansion, the term ②can be decomposed into infinite summation:

$$e^{\frac{-j4\pi d_{r,m}\sin\left(2\pi f_b t_q \varphi\right)}{\lambda}} = \sum_{n=-\infty}^{n=+\infty} (-1)^n J_n(z) e^{j2\pi n f_b t_q} e^{jn\varphi} \quad (17)$$

where $z=4\pi d_{r,m}/\lambda$, $J_n(z)$ is nth order Bessel function with arguments z. It can be found there are countless harmonics at nf_b in addition to the spectral lines at the breathing frequency f_b. Fortunately, $J_n(z)$ will decay rapidly when $|n|\geq 2$, so (12) can be approximated as:

$$e^{\frac{-j4\pi d_r \sin\left(2\pi f_b t_q+\varphi\right)}{\lambda}} \approx \sum_{n=-1}^{n=+1} (-1)^n J_n(z) e^{j2\pi n f_b t_q} e^{jn\varphi} \quad (18)$$

which consists of two spectral lines at $\pm f_b$ with respect to n = ±1 as well as a DC component with respect to n = 0. Combining (15) and (18), the zero-frequency components are mainly composed of static object reflections and decomposed zero-frequency components. These signals produce a significant peak in the frequency spectrum that affect the estimation of the target respiratory rate. We compute the mean in the sliding window and remove it to suppress static interference. At the same time, the Hamming window is used to prevent spectrum leakage. The AFM can be expressed as:

$$A(\theta, f) = \left| \sum_{q=1}^{Q} \left(\left(y(\theta, t_q) - \bar{y}(\theta, t_q) \right) \circ W_{\text{ham}}(Q) \right) e^{-j2\pi f \frac{q}{Q}} \right| \quad (19)$$

where $\bar{y}(\theta, t_q)$ is the mean of the data in the sliding window, Q is the length of the sild window, W_{ham} is the Hamming window and ∘ is Hadamard product. We compared AFM with and without removal mean as shown in the Fig. 5. It can be found that the proposed method can effectively suppress the interference of static clutter.

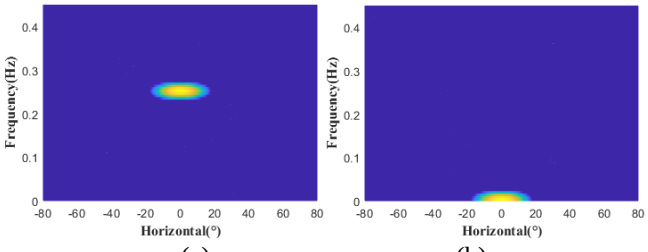

(a) (b)

Fig. 5. Experimental results with subject A at 2 m and 0°. (a)AFM spectrum with mean removal. (b) AFM without mean removal.

E. Sensing Capability Analysis

It is important to know under what conditions the proposed method can separate each target. In other words, we need to determine the spatial resolution and frequency resolution of the proposed method, which will help us design the perceptual system.

Assuming that different targets have different spatial positions, we use the targets' AOA to distinguish multiple targets. The discrimination capability in space domain depends on the half-power beamwidth. As described in Section II C, TMA can reconstruct conventional ULA. Then, the half-power width of the proposed system can be represented as:

$$\text{BW}_{3\text{dB}} = \frac{1}{\cos\theta} \frac{50.8\lambda}{Nd}(^\circ) \quad (20)$$

where θ is the steering angle, N denotes the element number of the ULA, d is the distance of two adjacent antenna units. The larger the number of antenna units, the narrower the beamwidth, the stronger the capacity of the array resolution spatial signal.

In addition, we also used the target breathing rate difference to separate multiple subjects. In practice, the ability to discriminate in the frequency domain depends on the frequency resolution, which is the minimum frequency separation on the frequency axis. Assuming that the sampling frequency is f_s, the number of sampling points is Q, and the sampling time is t, the frequency resolution Δf is expressed as:

$$\Delta f = \frac{f_s}{Q} = \frac{1}{t} \quad (21)$$

It can be found that the frequency resolution can be improved by increasing the sampling time.

It is worth noting that the proposed method joints the spatial and frequency domains. The complementary nature of multi-domain conjoint analysis can improve the performance of the system. If one domain's separation method fails, another mechanism may still work.

III. Results and Discussions

A. Experimental Setup

1) *Environment*: The experiments are conducted in two different scenarios with dimensions 7 m×7 m and 3 m × 2.5 m as shown in Fig.6 (b) and Fig. 9 (b), respectively. In order to evaluate the respiratory monitoring performance of the system, we performed extensive experiments in the first scenario and verified the anti-interference ability of the system in the second scenario.

2) *TMACW Parameter Settings*: The flow graph built by GNURadio configures the USRP as a 2.4GHz CW radar with a sampling rate of 200 KHz. Both the Tx gain and the Rx gain are 60 dB, and the Tx power is -17 dBm. The STM32 is used to generate the modulation function with a modulation period of 0.5 ms to control the RF switch according to Fig. 3, which means that the frequency interval between harmonics is 2 KHz. The distance between two adjacent antennas in the TMA is half a wavelength. The distances from the Tx antenna and the TMA to the ground are 70 cm and 85 cm, respectively. The USRP sends the collected data to a laptop with Intel i7-8700 CPU and 16 GB RAM via USB 3.0. The baseband signal processing is implemented in MATLAB 2020b. In harmonic recovery, the maximum extracted harmonic order K is equal to 2 to satisfy the full rank of the $\mathbf{\Gamma}$ matrix. We use the Filter Designer app of MATLAB to design the low-pass filter in

DDC with a passband of 0~50 Hz. The specific parameters of the TMACW radar are shown in Table I.

Table I
TMACW RADAR PARAMETERS

Parameters	Values
Carrier frequency f_c	2.4 GHz
Sampling frequency f_s	200 KHz
Modulation Period T_p	0.5 ms
USRP Tx gain	60 dB
USRP Rx gain	60 dB
Rx Antenna number	4
Tx antenna number	1
Gain of antenna	6 dB
Harmonic order K	2
Antenna space	6.25 cm
Time	30 s
Tx power	-17dBm

3) *Participants*: A total of 4 healthy volunteers participated in this study, i.e., aged from 23 to 29. The basic information of all volunteers is listed in Table II. During the experiment, slight movements of the head and limbs were allowed.

Table II
BASIC INFORMATION OF VOLUNTEERS

Volunteers	1	2	3	4
Gender	Male	Male	Male	Male
Age (year)	26	23	26	29
Height (cm)	176	177	181	180
Weight (Kg)	66	82	65	77
Width (cm)	30	34	32	33

4) *Ground-Truths:*
During the experiment, we asked the subjects to wear a piezoelectric breathing belt (HKH-11C) as the ground truth to evaluate the performance of the proposed TMACW radar. Except for the abnormal breathing detection experiment, all volunteers kept breathing naturally according to their habits.

B. Two-person Respiratory Detection with Angle Location and Beamforming

In this experiment, two subjects keep the same breathing rate as far as possible at angle 30° and -30° of the TMACW radar. The longitudinal distance between the subjects and the radar is 2 m. After processing by the proposed method, we can find that there are two highlighted parts in the AFM corresponding to object A and object B, as shown in Fig. 6(a). The AOA of the two subjects is -27.5° and 28°. The breathing frequency of both subjects is approximately 0.19 Hz. It can find that the AOA measured value deviates from the true value. The main reason is that people have a certain width and cannot be regarded as an ideal point target. In order to obtain the respiration time domain signal, we used conventional beamforming to generate two beams directed at subject A and subject B, respectively as shown in Fig. 6(c) and Fig. 6(e). The extended differentiation and cross-multiplication algorithms are used to obtain the respiration signal in the time domain to prevent phase ambiguity [48]. The difference in respiration amplitude may stem from the fact that the radar measures the signal containing both chest wall and abdominal displacement, whereas the breathing belt measures the displacement of the abdomen. The measured respiration rate is highly consistent with the ground truth as shown in Fig. 6(d) and Fig. 6(f).

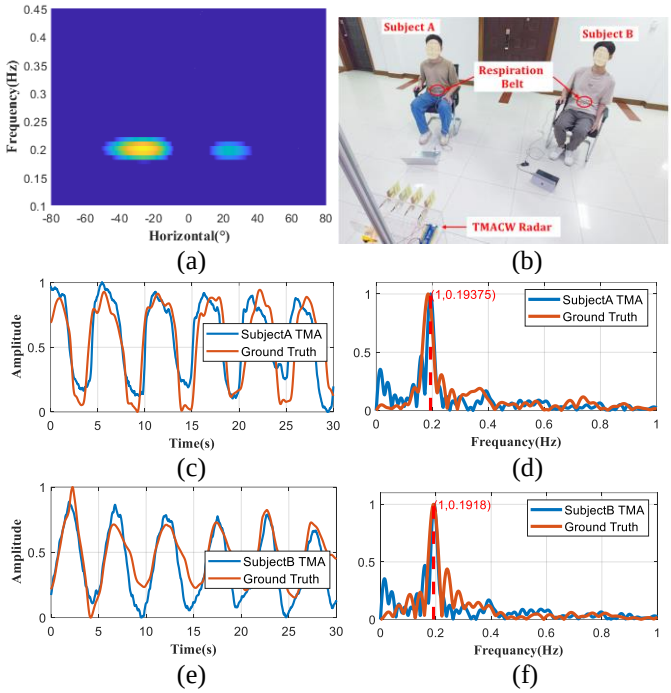

Fig. 6. Experimental results with Subject A at 2 m and -30◦ and Subject B at 2 m and 30◦. (a)AFM of two people monitoring. (b) Experimental setup. (c) The respiratory signal of subject A. (d) The spectrum of subject A. (e) The respiratory signal of subject B. (f) The spectrum of subject B.

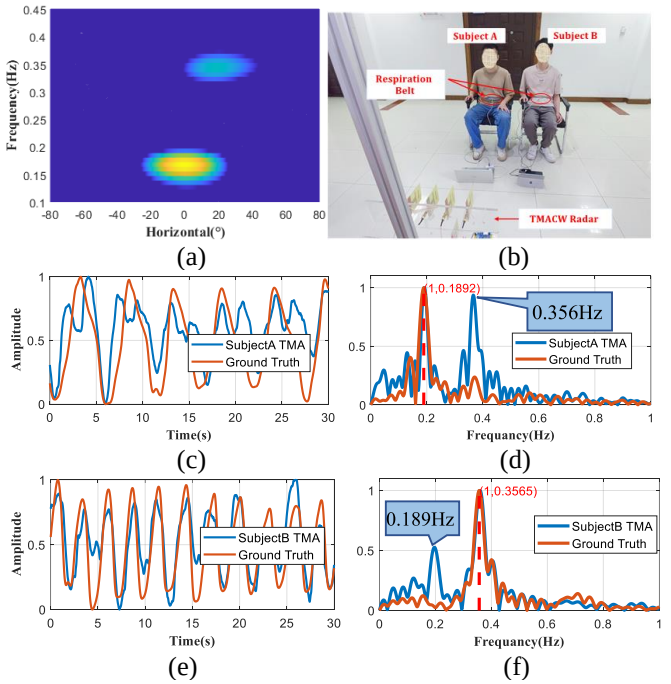

Fig. 7. Experimental results with Subject A at 2 m and 0◦ and Subject B at 2 m and 15◦. (a) AFM of two people monitoring. (b) Experimental setup. (c) The respiratory signal of subject A. (d) The spectrum of subject A. (e) The respiratory signal of subject B. (f) The spectrum of subject B.

According to Section II E, the spatial resolution of the proposed 4-element TMACW radars is 25 °. If the angle of the two subjects relative to the radar is less than 25°, the two targets cannot be separated from the spatial spectrum. If the difference between the breathing frequencies of the two targets is greater than the frequency resolution, we can distinguish them by the frequency spectrum. We set the length of the sliding window as 30 s, so Δf =0.03 Hz. In this experiment, two subjects are located at 0° and 15° of the radar, respectively, as shown in the Fig. 7(b). We asked subject B's breathing rate to be greater than that of subject A. It can be found that subject A and subject B correspond to (1°, 0.19 Hz) and (18.5°, 0.355 Hz) in the spectrum, respectively, as shown in the Fig. 7(a). Due to the wide beam produced by conventional beamforming, the respiration signal and spectrum of the two subjects will interfere with each other as shown in the Fig. 7 (c), (d), (e) and (f). The experimental results show that the multi-domain joint analysis makes up for the deficiency of the single-domain resolution and improves the performance of the system.

C. Abnormal Breathing Detection of Two Persons

The experimental setup is shown in Fig. 6(b). We asked subject A and subject B to simulate an apnea event within the first 30 s and the last 30 s, respectively. The Fig. 8 shows the breath signals of two subjects in one minute. Apnea events are marked by red boxes. In Fig. 8(b), we can clearly see that subject A has an apnea from 8s to 18s, and subject B has an apnea between 38s and 50s. From the above results, it can be seen that our system can not only detect multi-target breaths, but also detect abnormal breaths.

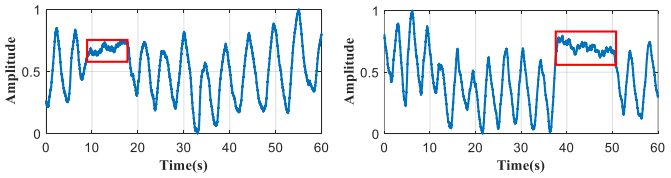

Fig. 8. Experiment of detecting abnormal breathing. (a) The respiratory signal of subject A. (b) The respiratory signal of subject B.

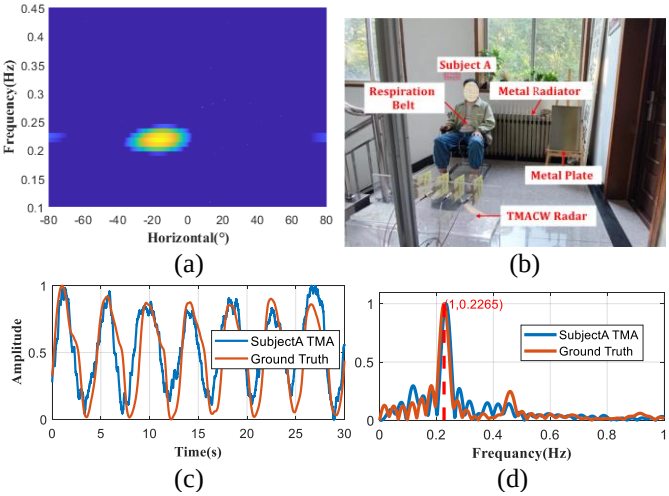

Fig. 9. Experimental results with Subject A at 2 m and -20◦. (a) AFM under multipath. (b) Experimental setup. (c) The respiratory signal of subject A. (d) The spectrum of subject A.

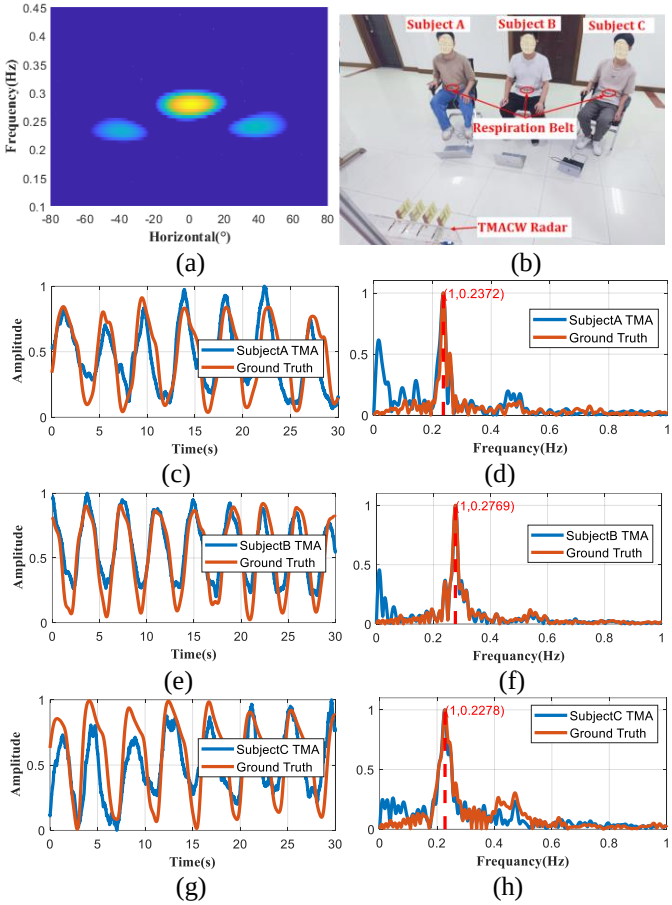

Fig. 10. Experiment of monitoring three subjects' respiration. (a) AFM of three people monitoring. (b) Experimental setup. (c) The respiratory signal of subject A. (d) The spectrum of subject A. (e) The respiratory signal of subject B. (f) The spectrum of subject B. (g) The respiratory signal of subject C. (h) The spectrum of subject C.

D. Impact of Strong Scatterers

If there are strong scatterers in the environment, the method based on AOA estimation may have false targets or interested targets submerged in the background noise. The larger the radar cross section (RCS) of the target, the stronger the echo. The RCS of metal is much larger than that of human. In order to verify the anti-interference ability of the proposed method, we conducted experiments in a complex environment with strong scatterers. The metal plate and the metal radiator are used as false targets, and the subject is located at the 30° of the radar as shown in the Fig. 9(b). The respiratory rate and position of the subjects can be clearly found on the AFM as shown in Fig. 9(a). It is worth noting that the information of the subject will not be affected by the metal plate and the metal radiator. In addition, the respiratory signal measured by the radar is consistent with the respiratory bandage as shown in Fig.9 (c) and Fig. 9(d).

E. Three-Person Respiratory Detection with Angle Location and Beamforming

In this experiment, we aim to explore the system capability in monitoring the number of targets. Three subjects were located at -30°, 0° and 30° of the radar. The distance from each subject to the radar is 2 m. The experimental scene is shown in Fig. 10(b). It can find three highlighted parts in the

AFM as shown in Fig. 10(a). Subject A, subject B and subject C correspond to (-36.5°, 0.238 Hz), (3°, 0.277 Hz) and (35°, 0.227 Hz) respectively. Based on the estimated AOA, beams directed towards each target are generated to obtain their respiration time domain signals as shown in the Fig. 10(c), (e) and (g). The breathing frequency of the three subjects are 0.2372 Hz, 0.2769 Hz, and 0.2278 Hz, respectively. The experimental results show that the respiration results measured by the TMACW radar are highly consistent with the respiration belt measurements.

F Performance of RR Estimation

In order to evaluate the performance of the proposed system, we conducted extensive experiments to statistically analyze the respiratory accuracy and error of the system. Specifically, we conducted experiments at different distances (1 m, 2 m, 3 m) and different numbers of subjects (1,2,3). Each experiment lasted 30 s and was repeated 15 times. A total of 135 samples were collected.

1) *Error Statistics*

Fig. 11(a) shows the cumulative distribution functions (CDF) of estimation error in RR estimation. It can be seen that the maximum RR estimation errors of the proposed system in single-person, two-person, and three-person scenarios are 0.77 bmp, 0.96 bmp, and 1.32 bmp, respectively. At the same time, we can find that 90% of the data has an estimated error under 0.9 bpm. The root mean square error (RMSE) is adopted to evaluate the robustness of the system under different numbers of subjects as shown in Fig.11(b). As the number of subjects increases, the RMSE increases slightly.

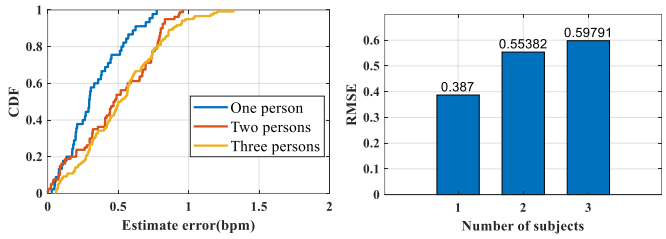

Fig. 11. (a) CDF of estimation error in RR estimation. (b) RMSE in RR estimation.

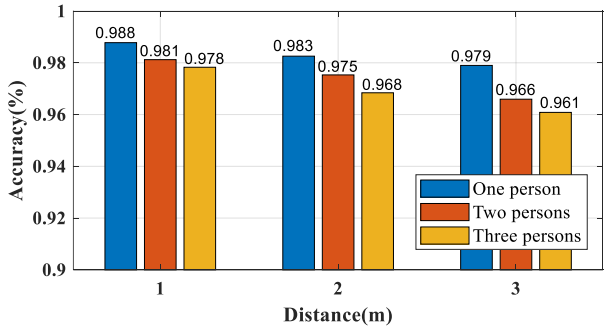

Fig. 12. Accuracy at various distances.

2) *Impact of Distance*

Fig. 12 presents the accuracy of RR sensing with different distances. The accuracy is calculated as: Accuracy $=1-\frac{1}{N}\sum\frac{|RR_{est}-RR_{ref}|}{RR_{ref}}$. As the number of subjects increases, the accuracy decreases slightly. When the distance between the TMACW radar and the subject increases, the subjects' echo energy decreases, which leads to a decrease in the SNR of the respiratory signal and accuracy of the estimated RR. It is worth noting that the average accuracy of RR for three people only drops slightly from 97.8% at 1m to 96.1% at 3m. These results demonstrate that the proposed system can accurately measure the respiratory rate of multiple people within 3m.

3)*Consistency Analysis*

In order to obtain accuracy, we calculated the Bland-Altman plot and Pearson correlation coefficient (r) with all the collected data. In the Bland–Altman analysis, the mean difference (MD) and standard deviation (SD) of the MD are the estimated bias and the average deviation from the MD, respectively. The 95% limits of agreement (LoA) are defined as MD ± 1.96 SD. In Fig. 13 (a) and (b), the blue dots, red dots, and yellow dots are samples for single-person, two-person, and three-person scenarios, respectively. The MD and SD of RR are -0.003 and 0.551. As shown in Fig. 10(a), the upper LoA and lower LoA are 1.077 bmp and -1.083 bmp, respectively. Only 4 samples exceeded LoA. The correlation coefficient r between the measured RR and the reference RR is as high as 1.0008 as shown in Fig.13 (b). In summary, the proposed system has high consistency with medical sensors and has the potential to replace wearable devices.

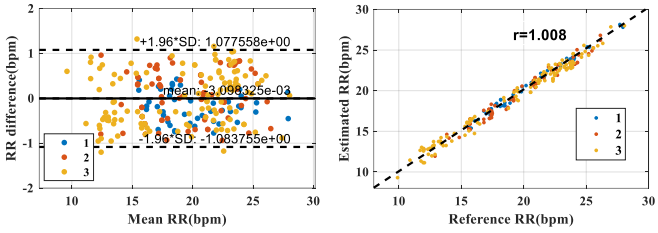

Fig. 13. Consistency analysis. (a) Bland-Altman of the estimated RR. (b) Scatter plot of the estimated RR.

G. Comparison with Other Relevant Works

Table III compares state-of-the-art sensing technologies for vital sign detection. It can be observed that our approach is very different from previous research in terms of sensing devices and signal processing methods. In [4], the author mainly focuses on low power to meet long-term monitoring needs. In [9], the study aims to reduce mutual coupling interference. Unfortunately, multi-person monitoring has not been emphasized in these studies. WiFi devices have the advantages of integrated communication sensing and low cost. The method of frequency separation cannot separate subjects with the same RR and obtain time-domain signals of vital signs [14]. The time-division radar obtains spatial information to separate multiple targets [28,35,36]. However, strict synchronization between the receiver and the switch is required, which means that the received signals need to be divided into each transceiver link. The proposed system does not require strict synchronization and can convert the TMA into the conventional array through harmonic recovery. Compared to radar with wideband, the proposed system has lower spectrum occupancy and transmission power. Compared to multi-channel radar [33-35], The proposed system achieves the same performance using fewer antennas. In addition, the

multi-domain joint estimation method can improve the anti-interference ability of the system and reduce misjudgment.

TABLE III
PERFORMANCE COMPARISON OF OUR SYSTEM WITH THE STATE-OF-ART RESEARCH

REF#	Tech.	Tx freq. (GHz)	Tx/Rx antenna	Tx/Rx channel	Vital Sign	Sampling Rate (Hz)	Tx power (dBm)	Max. Range (m)	Min. radial dis. between subjects (m)	No. of subjects	Min. Angle (°)
[4]	MFCW	2 (75MHz)	1/1	1/1	RR	NA	-13.1	2	NA	1	NA
[9]	FMCW	77-81	3/4	3/4	RR/HR	2M	NA	1	NA	1	NA
[14]	WiFi	5.765 (40MHz)	1/3	1/3	RR	NA	20	NA	NA	5	NA
[19]	FMCW	5.46-7.25	1/1	1/1	RR/HR	NA	NA	8	1.5	3	NA
[21]	FMCW	5.72-5.82	1/1	1/1	RR/HR	20K	NA	2	0.7	2	NA
[25]	SFCW	2-3	1/1	1/1	RR/HR	48K	8	1.6	0.68	2	NA
[27]	SFCW	2-4	1/1	1/1	RR	15K	20	6.3	0.3	3	NA
[28]	SFCW	1.75–2.25	10/10	1/1	RR/HR	20([1]ST)	20	2.5	NA	3	NA
[29]	SFCW UWB	8.35-12.35 6-8.5	1/1 1/1	1/1 1/1	RR/HR	20(ST) 30(ST)	0	2.3	0.1	3	NA
[30]	SIL+ Thermal Camera	2.3-2.65	2/2	2/2	RR/HR	NA	0	4	NA	5	NA
[31]	LWA SIL	1.85-2.85	1/1	1/1	RR/HR	125KHz	-2-6	1	0.52	2	30
[33]	Phased array	2.4	4/4	4/4	RR/HR	NA	0	6	NA	2	NA
[34]	SIMO CW	5.8	1/8	1/8	RR	200K	8	3	0	3	15
[35]	MIMO CW	2.4	6/6	6/6	RR/HR	50K	0	1.8	0	2	17
[36]	SIL FMCW	5.8-6.8	1/8	1/1	RR/HR	64	5	4	0	5	NA
[37]	FMCW	77-81	2/4	2/4	RR/HR	2M	12.5	NA	NA	3	17.5
This work	**TMA CW**	2.4	1/4	1/1	RR	200K	-17	3	0	3	15

[1]ST means slow time

H. Discussion

There are several limitations in this study. First, it is very difficult for the proposed system to detect heartbeat signals from multiple people. The reason is that when converting beams into the frequency domain, the weak heartbeat signals are easily submerged in the respiratory harmonics and noise. It is difficult to observe heartbeat signals in AFM. Second, the 4-element TMA receiving array has a low spatial resolution. Although it is possible to distinguish two adjacent targets depending on frequency resolution, the extracted breath signal is subject to interference from adjacent targets. Third, it is difficult to detect respiratory signal when a moving object is obstructed in front of the subject. The reason is that the moving object introduces dynamic components whose strength is much greater than the echo of the target behind it. Vital sign signals drown in the interference and can't be detected. Finally, our system can only utilize beam scanning in the plane. When the system is applied in hospital scenarios, it is necessary to change the deployment location of the system.

The proposed TMCW radar has other potential applications besides respiratory detection. Our system has the advantage of low Tx power so it can be used for long-term sleep monitoring. In addition, the proposed system has the same function as the conventional multi-channel radar. By combining Doppler information and angle information, the system can realize gesture recognition, user identification and fall detection.

IV. CONCLUSION

In this paper, A novel single-channel TMACW radar is proposed to enable multi-person respiratory sensing. The radar consists of a 4-element Rx TMA and one Tx antenna. The harmonics generated by time modulation are utilized to recover the conventional array signals which reduces the hardware complexity of multi-channel radars. We also propose a joint spatial and frequency domain method to estimate the AOA and RR of multiple targets simultaneously. The experimental results show that the proposed system has high consistency with the reference sensor. Although the proposed system still has some limitations such as lack of HR estimation capability, number of detected targets, and inapplicability to moving object occlusion scenarios, it is foreseeable that the optimization of radar hardware and algorithms will also attract more researchers' attention. We also believe that the proposed radar can be considered a promising sensing technology for long-term health monitoring in the future.

REFERENCES

[1] M. Folke et al., "Critical review of non-invasive respiratory monitoring in medical care," *Med. Biol. Eng. Comput*., vol. 41, no. 4, pp. 377–383, 2003.
[2] G. Scebba, G. D. Poian, and W. Karlen, "Multispectral video fusion for non-contact monitoring of respiratory rate and apnea," *IEEE Trans. Biomed. Eng.*, vol. 68, no. 1, pp. 350–359, Jan. 2021.
[3] F. Deng et al., "Design and Implementation of a Noncontact Sleep Monitoring System Using Infrared Cameras and Motion Sensor," *IEEE Trans.*

Instrum. Meas., vol. 67, no. 7, pp. 1555-1563, July 2018.
[4] H. Zhao et al., "Noncontact Physiological Dynamics Detection Using Low-power Digital-IF Doppler Radar," *IEEE Trans. Instrum. Meas*., vol. 66, no. 7, pp. 1780-1788, July 2017.
[5] J. C. Y. Lai et al., "Wireless Sensing of Human Respiratory Parameters by Low-Power Ultrawideband Impulse Radio Radar," *IEEE Trans. Instrum. Meas*., vol. 60, no. 3, pp. 928-938, March 2011.
[6] I. Kakouche et al., "Fast and cost-effective method for non-contact respiration rate tracking using UWB impulse radar," *Sens. ActuatorsA, Phys.*, vol. 329, Oct. 2021, Art. no. 112814.
[7] J. Tu and J. Lin, "Fast Acquisition of Heart Rate in Noncontact Vital Sign Radar Measurement Using Time-Window-Variation Technique," *IEEE Trans. Instrum. Meas*., vol. 65, no. 1, pp. 112-122, Jan. 2016.
[8] M. Xiang et al., "High-Precision Vital Signs Monitoring Method Using a FMCW Millimeter-Wave Sensor," *Sensors*, vol. 22, no. 19, p. 7543. Oct. 2022.
[9] X. Zhang, Z. Liu, Y. Kong and C. Li, "Mutual Interference Suppression Using Signal Separation and Adaptive Mode Decomposition in Noncontact Vital Sign Measurements," *IEEE Trans. Instrum. Meas*., vol. 71, pp. 1-15, 2022.
[10] G. Li et al., "Detection of Human Breathing in Non-Line-of-Sight Region by Using mmWave FMCW Radar," *IEEE Trans. Instrum. Meas*., vol. 71, pp. 1-11, 2022.
[11] M. Ascione et al., "A New Measurement Method Based on Music Algorithm for Through-the-Wall Detection of Life Signs," *IEEE Trans. Instrum. Meas*., vol. 62, no. 1, pp. 13-26, Jan. 2013.
[12] K. Wang, Z. Zeng and J. Sun, "Through-Wall Detection of the Moving Paths and Vital Signs of Human Beings," *IEEE Geosci. Remote Sens. Lett*., vol. 16, no. 5, pp. 717-721, May 2019.
[13] Y. Ma et al., "Non-Contact Vital States Identification of Trapped Living Bodies Using Ultra-Wideband Bio-Radar," *IEEE Access*, vol. 9, pp. 6550-6559, 2021.
[14] C. Chen et al., "TR-BREATH: Time-Reversal Breathing Rate Estimation and Detection," *IEEE Trans. Biomed. Eng.*, vol. 65, no. 3, pp. 489-501, March 2018.
[15] X. Wang, C. Yang and S. Mao, "Tensorbeat: Tensor decomposition for monitoring multiperson breathing beats with commodity WiFi," *ACM Trans. Intell. Syst. Technol*., vol. 9, no. 1, pp. 8:1-8:27, Sep. 2017.
[16] L. Ren et al., "Noncontact multiple heartbeats detection and subject localization using UWB impulse Doppler radar," *IEEE Microw. Wireless Compon. Lett*., vol. 25, no. 10, pp. 690–692, Oct. 2015.
[17] X. Dang, J. Zhang, Z. Hao, "A Non-Contact Detection Method for Multi-Person Vital Signs Based on IR-UWB Radar," *Sensors*, vol. 22, no.16, p. 6116, Aug. 2022.
[18] X. Shang, J. Liu, and J. Li, "Multiple object localization and vital sign monitoring using IR-UWB MIMO radar," *IEEE Trans. Aerosp. Electron. Syst.*, vol. 56, no. 6, pp. 4437–4450, Dec. 2020.
[19] F. Adib et al., "Smart homes that monitor breathing and heart rate," in *Proc. ACM CHI*, Apr. 2015, pp. 837–846.
[20] Z. Peng et al., "A portable FMCW interferometry radar with programmable low-IF architecture for localization, ISAR imaging, and vital sign tracking," *IEEE Trans. Microw. Theory Techn*., vol. 65, no. 4, pp. 1334–1344, Apr. 2017.
[21] G.-W. Fang, C.-Y. Huang, and C.-L. Yang, "Simultaneous detection of multi-target vital signs using EEMD algorithm based on FMCW radar," in *IEEE MTT-S Int. Microw. Symp. Dig.*, May 2019, pp. 1–4.
[22] H. Lee, B.-H. Kim, and J.-G. Yook, "Path loss compensation method for multiple target vital sign detection with 24-GHz FMCW radar," in *Proc. IEEE Asia–Pacific Conf. Antennas Propag. (APCAP)*, Aug. 2018, pp. 100–101.
[23] H. Lee et al., "A novel vital-sign sensing algorithm for multiple subjects based on 24-GHz FMCW doppler radar," *Remote Sens.*, vol. 11, no. 10, pp. 1–15, May 2019.
[24] M. Mercuri et al., "Vital-sign monitoring and spatial tracking of multiple people using a contactless radar-based sensor," *Nature Electron*., vol. 2, no. 6, pp. 252–262, Jun. 2019.
[25] S. Nahar et al., "An electromagnetic model of human vital signs detection and its experimental validation," *IEEE J. Emerg. Sel. Topics Circuits Syst*., vol. 8, no. 2, pp. 338–349, Jan. 2018.
[26] W.-C. Su et al., "Stepped-frequency continuous-wave radar with self-injection-locking technology for monitoring multiple human vital signs," *IEEE Trans. Microw. Theory Techn*., vol. 67, no. 12, pp. 5396-5405, 2019.
[27] Y. E. Acar, I. Saritas and E. Yaldiz, "An experimental study: Detecting the respiration rates of multiple stationary human targets by stepped frequency continuous wave radar," *Measurement*, vol. 167, Jan. 2021.
[28] Z. Li et al., "Through-Wall Multi-Subject Localization and Vital Signs Monitoring Using UWB MIMO Imaging Radar," *Remote Sens.*, vol. 13, no. 15, p. 2905, Jan. 2021.
[29] L. Qiao et al., "Learning-Refined Integral Null Space Pursuit Algorithm for Noncontact Multisubjects Vital Signs Measurements Using SFCW-UWB and IR-UWB Radar," *IEEE Trans. Instrum. Meas*., vol. 71, pp. 1-13, 2022.
[30] D. -M. Chian et al., "Vital Signs Identification System with Doppler Radars and Thermal Camera," *IEEE Trans. Biomed. Circuits Syst.*, vol. 16, no. 1, pp. 153-167, Feb. 2022.
[31] Y. Yuan et al., "Multi-target concurrent vital sign and location detection using metamaterial-integrated self-injection-locked quadrature radar sensor," *IEEE Trans. Microw. Theory Techn.*, vol. 67, no. 12, pp. 5429-5437, 2019.
[32] Y. Yuan and C. -T. M. Wu, "Super-Regenerative Oscillator Integrated Metamaterial Leaky Wave Antenna for Multi-Target Vital Sign and Motion Detection," *IEEE J. Electromagn. RF Microw. Med. Biol*. vol. 6, no. 2, pp. 238-245, Jun. 2022.
[33] M. Nosrati et al., "A concurrent dual-beam phased-array Doppler radar using MIMO beamforming techniques for short-range vital-signs monitoring," *IEEE Trans. Antennas Propag.*, vol. 67, no. 4, pp. 2390–2404, Apr. 2019.
[34] J. Xiong et al., "Multitarget respiration detection with adaptive digital beamforming technique based on SIMO radar," *IEEE Trans. Microw. Theory Techn*., vol. 68, no. 11, pp. 4814-4824, 2020.
[35] C. Feng et al., "Multitarget vital signs measurement with chest motion imaging based on MIMO radar," *IEEE Trans. Microw. Theory Techn*., vol. 69, no. 11, pp. 4735-4747, 2021.
[36] W. -C. Su et al., "2-D Self-Injection-Locked Doppler Radar for Locating Multiple People and Monitoring Their Vital Signs," *IEEE Trans. Microw. Theory Techn*., vol. 69, no. 1, pp. 1016-1026, Jan. 2021.
[37] Y. Wang et al., "Multi-target vital signs detection using frequency-modulated continuous wave radar," *EURASIP J. Adv. Signal Process*, vol. 2021, no. 1, pp. 1-19, 2021.
[38] W. F. Wang et al., "MmHRV: Contactless heart rate variability monitoring using millimeter-wave radio," *IEEE Internet Things J.*, vol. 8, no. 22, pp. 16623–16636, Nov. 2021.
[39] Chen, S. Lan and G. Zhang, "Multiple-Target Vital Signs Sensing using 77GHz FMCW radar," in *Proc. 15th Eur. Conf. Antennas Propag. (EuCAP)*, , Mar. 2021, pp. 1–3.
[40] Y. Zeng et al., "MultiSense: Enabling multi-person respiration sensing with commodity WiFi", *Proc. ACM Interact. Mobile Wearable Ubiquitous Technol.*, vol. 4, no. 3, pp. 1-29, Sep. 2020.
[41] S. Yue et al., "Extracting multiperson respiration from entangled RF signals," in *Proc. ACM Interact. Mob. Wearable Ubiquitous Technol. (IMWUT)*, vol. 2, no. 2, Jul. 2018, pp. 1-22.
[42] L. Zhang et al., "Noncontact MultiTarget Respiration Sensing Using SIMO Radar With UBSS Method," *IEEE Microw. Wireless Compon. Lett*., pp. 1–4, 2022.
[43] H. E. Shanks and R. W. Bickmore, "Four-dimensional electromagnetic radiators," *Can. J. Phys*., vol. 37, no. 3, pp. 263-275, 1959.
[44] W. T. Li, Y. J. Lei and X. W. Shi, "DOA estimation of time-modulated linear array based on sparse signal recovery," *IEEE Antennas Wirel. Propag. Lett.*, vol. 16, pp. 2336-2340, 2017.
[45] G. Huang et al., "Target Localization Using Time-Modulated Directional Modulated Transmitters," *IEEE Sensors J.*, vol. 22, no. 13, pp. 13508-13518, 2022.
[46] S. Prager et al., "Ultrawideband synthesis for high-range-resolution software-defined radar," *IEEE Trans. Instrum. Meas*., vol. 69, no. 6, pp. 3789–3803, Jun. 2020.
[47] W. Feng, J. M. Friedt, and P. Wan, "SDR-Implemented Ground-Based Interferometric Radar for Displacement Measurement," *IEEE Trans. Instrum. Meas.*, vol. 70, pp. 1-18, 2021.
[48] J. Wang et al., "Noncontact distance and amplitude-independent vibration measurement based on an extended DACM algorithm," *IEEE Trans. Instrum. Meas*., vol. 63, no. 1, pp. 145–153, Jan. 2014.